Role of the tip atom in STM and AFM: Theory of atom transfer

E. Koetter
Ludwig-Maximilians-Universität, München, Germany

D. Drakova
University of Sofia, Sofia, Bulgaria

G. Doyen
Ludwig-Maximilians-Universität, München, Germany

(Received 20 March 1995; revised manuscript received 20 February 1996)

The interaction energy and forces between tunnel tips composed of an adsorbed W or Al atom on W(110) and Al(111) with an Al(111) sample surface have been calculated within a spin-unrestricted screened Hartree-Fock theory, which includes electron correlation, multiple image effects, and the electric fields between tip and sample. The potential-energy surface for an Al atom between the W(110) and the Al(111) electrodes is also calculated within the same model. The results show that the Al atom will be spontaneously transferred from the Al surface to the W surface, if the W(110) surface is brought close enough to the Al(111) electrode. This suggests that transfer of Al atoms to the tip in scanning tunneling microscopy will occur, if an Al(111) surface is scanned with a tungsten tip. The analysis of the interaction energy between the tip and the sample reveals the physics behind this behavior. The special properties of the Al/W(110) tip formed in this way are discussed in relation to the tunnel current and the force gradient, which have been measured by Dürig and Züger for an Ir tip on an Al foil. The calculated force gradients for the Al/W(110) tip above the Al(111) sample surface resemble closely the experimental results of Dürig and Züger, indicating that material transport from the sample to the tip has occurred in these experiments. The force between the tip and sample reaches its attractive extremum at a relatively large tip-sample separation of 8 Å and the force gradient changes sign because the dominating interaction changes from the long-range image type to chemisorption covalentlike. With the tunnel tip obtained by Al-atom transfer from the Al(111) surface to the W(110) electrode, the theory gives a satisfactory explanation of the trends displayed by the measured tunnel current and the force gradient. Comparison of the theoretical and the experimental force gradient provides the possibility of calibrating the absolute tip-sample distance. [S0163-1829(96)01224-6]

I. INTRODUCTION

Atomic scale manipulation of the tunnel tip and the sample surface in scanning tunneling microscopy (STM) is gaining importance in view of its potential to produce surface structures on the nanometer scale. Aside from the technological interest, the manipulation of the tip in a usually not very well defined way has interesting consequences for the STM imaging *per se*, e.g., it leads to atomic resolution, changes the distance dependence of the tunnel current, and even produces image inversion, where protrusions turn into indentations and vice versa. It has often been suggested by experimentalists that (field-induced) mass transport and diffusion may occur in a STM operation, modifying both the sample surface and the tunnel tip in an uncontrolled way.[1–5]

By means of manipulations with the tunnel tip and the bias voltalge, it proves possible to transfer single atoms or atom clusters from the sample towards the tip and to place them with precision on the scale of atomic dimensions back on the sample surface.[3–5] This is possible in the low temperature STM at 4 K when the surface atom diffusion does not interfere and under ultrahigh vacuum conditions. In the experiments of Eigler and co-workers,[3,4] a voltage pulse of positive or negative sign is applied relative to a Ni(110) sample, leading to the reversible transfer of an adsorbed Xe atom in the direction of the tunnel current. In the experiments of Lyo and Avouris,[5] even at room temperature Si atoms or clusters could be removed and deposited on the STM tip or vice versa in the direction opposite to the direction of current flow. Another example is the transfer of Au clusters from a gold tip towards the sample at voltages above some threshold value.[2]

The physics of the transfer of adsorbed atoms, due to the applied external electric field, has been studied by Kreuzer, Wang, and Lang[6] by Lang,[7] by Walkup, Newns, and Avouris,[8] by Gao, Persson, and Lundqvist,[9] and recently by Brandbyge and Hedegård,[10] and by Hirose and Tsukada.[11] The driving mechanism usually discussed involves field evaporation combined with the effect of the chemical tip-sample interaction forces.[6,7] In these cases (transfer of Xe or Si atoms) strong external electric fields and the modification of the barrier for field-induced atom or ion desorption are important. Other mechanisms of atom transfer are atom tunneling and thermally activated transfer, as discussed by Gomer.[12] In the paper by Dürig *et al.*,[13] empirical nearest-neighbor two-body potentials are constructed, which are then summed up to get the interaction energy between an Ir-tip cluster and a cluster of Al atoms describing the Al(111) face. They achieve good agreement with the experiments, but this approach is not capable of revealing the underlying physics.

Except for the fact that they find that an aluminum atom transferred towards the Ir-tip cluster reproduces the experimental force gradients, we cannot find any other connection to our work. Our own studies showed that two-body potentials are not capable of reproducing the many-particle potentials over the whole physically relevant range of distances.[14]

We study the transfer of a *metal atom* (which has a completely different electronic structure compared to the Xe or Si) in the absence of an external electric field. In this case, the atom follows the gradient of the potential-energy surface. Ciraci[15] has discussed this situation for the case of two Al(100) electrodes with an Al atom in between. The results (based on super cell calculations in the local-density approximation) are in good qualitative agreement with ours, where they are comparable. Our investigation extends these studies by (a) considering an atom between two *different* electrodes (different chemical nature and different lattice structure), (b) explicitly including the multiple image interactions, (c) performing a detailed analysis of the tip-sample interaction energy, and (d) calculating the tunneling current in addition to the interaction energies and forces. Energies and forces acting on a single Al-tip atom between two flat electrodes W(110) and Al(111) and the interelectrode forces are reported. The internal electric field, due to difference in the work functions of the two surfaces, is accounted for. The results show that the Al atom is spontaneously transferred from the Al surface towards the W surface at closer distance. The activation barrier for atom transfer collapses, due to the chemical interactions in the system.

The calculated force gradient for a rigid Al/W(110) tip above the Al(111) sample surface resembles closely the experimental results of Dürig and Züger[16] for an Ir tip on an Al film, indicating that material transport from the sample to the tip has occurred in these experiments. Dürig and Züger[16] measured, in addition to the tunnel current, simultaneously, the force gradient as a function of tip-sample separation. In the case of transition metal samples, the interaction force could be measured within the range of distances where the attractive component dominates as repulsion occurs at too small distances. For an Al film the situation was, however, qualitatively different. The force gradient was found to be an order of magnitude smaller than for transition metal samples and it turned to positive values at distances that correspond to typical tunneling conditions. Our aim is not so much to reproduce the measured values for a special tip/sample system, but to understand the trend in the described experiments in physical terms.

An appropriate interpretation of the experimental findings poses the challenge to the theory of STM to evaluate within the same model the electronic structure, the interaction forces, and the tunnel current for a realistic tunnel junction, including a tip that is truly three-dimensional and includes *d* electrons. First principle methods are not yet in a shape to tackle this difficult task, but careful model studies can already yield valuable information and add to the understanding of this important subject.

For several reasons, first principle methods based on the local-density approximation cannot be used to solve this complicated problem of two semi-infinite metal electrodes with the atomic structure being in contact with each other via a tip atom.

(1) The two plane electrodes consisting of a W(110) and an Al(111) surface have different geometry and unit cells, which prevents the use of supercell methods, because of the lattice mismatch. In addition, the introduction of the tip atom will break any kind of symmetry. Any kind of supercell calculation will introduce an array of tips with artificial tip-tip interactions.

(2) In order to calculate the tunnel current, one has to treat two semi-infinite metal electrodes.

(3) The local-density approximation does not treat the image interaction correctly, which is essential for obtaining a realistic barrier potential and which has an important influence on the magnitude of the tunnel current and the interaction potential.

(4) First principle methods use basis sets (e.g., plane waves, floating Gaussians, etc.), which are optimized to obtain numerically correct numbers, but which are not physically significant expansions in the sense that they facilitate a quantitative interpretation of the nature of the tip-sample interaction.

The fundamental physical phenomena can be qualitatively understood without having the exact first-principle solution available, if the interactions and self-energies are modeled carefully, based on the available knowledge and physical intuition. In the next section, a brief description of the theoretical model and the applied method of solution is given. Section III describes three different tunnel tips. The potential-energy curves and the analysis of the chemisorption bond between the tip atoms and the tip base metal reveal the different nature of the bonding of an Al-tip atom compared to a W-tip atom on W(110). In Secs. IV and V, a similar analysis is performed for the interaction energy of the tips with the Al(111) surface. The total-energy surface of an Al atom between W(110) and Al(111) reveals the collapse of the activation barrier for atom transfer towards the tungsten surface and the nonactivated nature of the transition of an adsorbing aluminum atom from Al(111) towards W(110) below a certain interelectrode separation. This is a consequence of the stronger bonding of an Al atom to W(110), which is related to the presence of *d* electrons. The distance dependence of the tunnel conductivity and the force gradient between the Al(111) sample and the Al/W(110) tip produced in this way, compare nicely to the experimentally measured trends and support the picture of an Al atom being transferred towards the W tip in experiment. The results for the Al/Al(111) tip, presented in Sec. VI suggest that a similar behavior is expected if a whole cluster of Al atoms get transferred towards the tungsten tip.

II. THE MODEL

We consider the scanning tunneling microscope from the point of view of a single tip atom or a cluster of tip atoms adsorbed on a semi-infinite tip electrode, interacting with a semi-infinite sample surface. In the present work, the tip is treated as a metal atom (called tip atom) absorbed on a flat metal surface. Figure 1 summarizes some essential characteristics of the model Hamiltonian, which treats the local region near the tip atom in a quite explicit way. The interaction between the tip atom and the metal surfaces involves short-range and long-range effects. The short-range effects

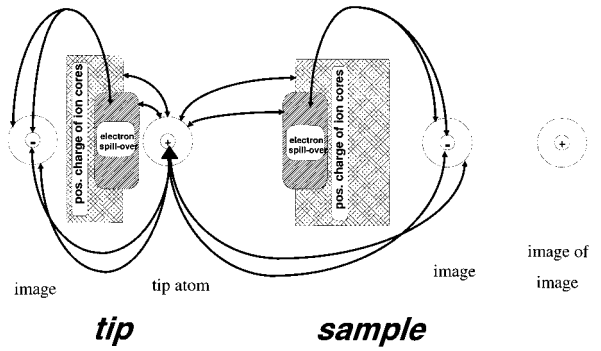

FIG. 1. Illustration of the interactions in the STM included in the Hamiltonian.

are calculated within the region overlapped by the tip atom wave functions and include electron-electron interactions and a potential due to the tip-atom core (V_{tipcore}). The attractive screened core potential as felt by the metal electrons is described as a generalized Göppert-Mayer-Sklar (GMS) potential (V_{GMS}). The screened tip core potential acting on overlap charges is of the Yukawa-type (V_{Yuk}). These potentials are tip orbital dependent and they are parametrically introduced in the model Hamiltonian. They have been extensively studied before.[17,18] The polarization of the more distant metal electrons leads to image effects, which can be handled by coupling the local charge density to surface and bulk plasmons. Multiple image effects arising from the polarization of one electrode by the induced charge density in the other electrode have to be included as well. Other interactions accounted for explicitly in the model Hamiltonian concern the metal surface dipole layer and the core-core repulsion.

A. The Hamiltonian

It is reasonable to partition the Hamiltonian according to the different geometrical regions as illustrated in Fig. 2:

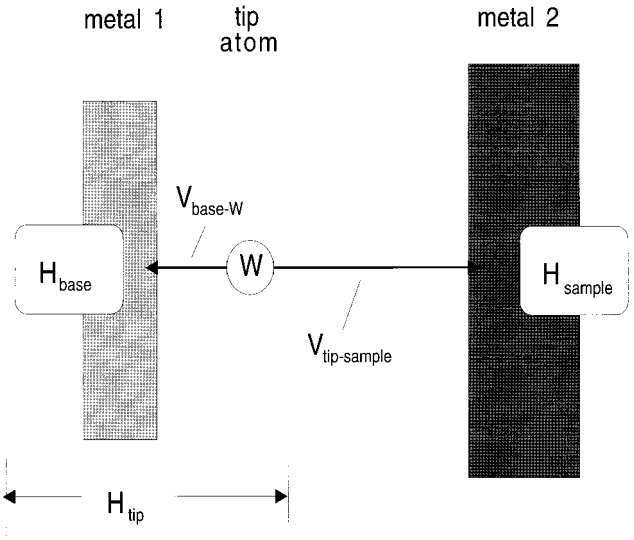

FIG. 2. Schematic representation of the STM Hamiltonian.

$$H = H_0 + V_{\text{tip -sample}} \tag{1}$$

$$= H_{\text{tip}} + H_{\text{sample}} + V_{\text{tip -sample}} \tag{2}$$

$$= H_{\text{base}} + V_{\text{atom -base}} + H_{\text{atom}} + H_{\text{sample}} + V_{\text{tip -sample}}\,. \tag{3}$$

H_0 describes the noninteracting tip plus sample surface. The tip is described by a tungsten atom or an Al atom adsorbed on a flat W surface. H_{atom} stands for the isolated tip-atom and H_{base} for the flat W surface. H_{sample} represents the sample surface without the tip present and $V_{\text{tip -sample}}$ is the interaction between the tip and the sample.

The explicit form of the model Hamiltonian (formulated in the notation of second quantization) is the following:

$$H_{\text{atom}} = \sum_{A,s} \langle As| -\tfrac{1}{2}\nabla^2 + V_{\text{tipcore}}|As\rangle n_{As} + \sum_{B,t\geqslant A,s} \langle AsBt|V_{\text{el -el}}|AsBt\rangle n_{As} n_{Bt}\,, \tag{4}$$

$$H_{\text{base}} + H_{\text{sample}} = \sum_{k,s} \langle ks| -\tfrac{1}{2}\nabla^2 + V_{\text{metcore}}|ks\rangle n_{ks} + \sum_{k,l,s} [\langle ks|V_{\text{GMS}}|ls\rangle a^\dagger_{ks} a_{ls} + \text{H.c.}]$$
$$+ \sum_{l,t\geqslant k,s;n,t\geqslant m,s} \langle kslt|V_{\text{el -el}}|msnt\rangle a^\dagger_{ks} a^\dagger_{lt} a_{ms} a_{nt}\,, \tag{5}$$

$$V_{\text{atom -base}} + V_{\text{tip -sample}} = \sum_{A,k,s} [\langle As| -\tfrac{1}{2}\nabla^2 + V_{\text{Yuk}} + V_{\text{metcore}}|ks\rangle a^\dagger_{As} a_{ks} + \text{H.c.}] + \sum_{A,B,k,s,t} [\langle AsBt|V_{\text{el -el}}|Askt\rangle n_{As} a^\dagger_{Bs} + \text{H.c.}]$$
$$+ \sum_{A,s;l,t\geqslant k,t} [\langle Askt|V_{\text{el -el}}|Aslt\rangle n_{\text{As}} a^\dagger_{kt} a_{lt} + \text{H.c.}] + \sum_{A,B,k,l,s,t} [\langle AsBt|V_{\text{el -el}}|kslt\rangle a^\dagger_{As} a^\dagger_{Bt} a_{ks} a_{lt} + \text{H.c.}]$$
$$+ \sum_{A,k,s,t;m,t\geqslant l,t} [\langle Aslt|V_{\text{el -el}}|ksmt\rangle a^\dagger_{As} a^\dagger_{lt} a_{ks} a_{mt} + \text{H.c.}] + V_{\text{core-core}} + H_{\text{plasmon}}\,. \tag{6}$$

$V_{\text{el-el}}$ is the Coulomb repulsion between electrons, V_{metcore} is the attractive potential of the tip base and sample ion cores. $V_{\text{core-core}}$ is the core-core repulsion. H_{plasmon} is the operator describing the interaction with the surface plasmons, which yields the long-range component of the interactions in the combined system.[19] A,B refer to the tip-atom basis orbitals, k, l, m, n label the unperturbed metal basis states, s, t assume the values $\uparrow$ and $\downarrow$ and refer to the z component (perpendicular to the surface) of the electron spin. a_{is}, $a_{jt}^{\dagger}$, and $n_{is}=a_{is}^{\dagger}a_{is}$ denote the electron destruction, creation, and number operators, respectively.

Equations (4)–(6) contain a full set of one- and two-electron integrals. This allows us to account for all important physical interactions like electron-core attraction, electron-electron repulsion, and core-core repulsion. The interaction of an atom with a single metal surface is just the chemisorption problem that is routinely handled by this method. The metal surfaces are semi-infinite and have atomic structure.

B. Parametrization

The model Hamiltonian (MH) is set up and parametrized to satisfy the following general criteria.

(i) The ''model space,'' in which the MH is defined, is a subset of the total Hilbert space. It should be accessible to physical intuition, i.e., it should be adapted to the chemical constituents from which the system is built.

(ii) The MH should yield sufficiently accurately the low-lying part of the exact energy spectrum.

(iii) The model space should be complete enough to avoid intruder states.

(iv) The interaction terms, though simplified, should be mutually and physically consistent to avoid artifacts like ghost states, electron nonconservation, etc.

(v) Transferrability of potentials and parameters should be guaranteed.

According to the above criteria, the electronic structure of the separated system (tip base, sample surface, and the isolated tip atom) is not recalculated, but is taken from *ab initio* calculations and reliable experimental information is used to compensate for errors like neglected correlation effects.

The one- and two-electron integrals in Eqs. (4)–(6) are reexpressed in terms of overlap integrals and a handful of Coulomb repulsion integrals, exchange integrals, and core energies on the tip atom.[18] The latter are determined by solving a system of equations, so that the experimentally determined ionization and affinity energies are reproduced. This is described in Ref. 35. The overlap integrals are evaluated numerically from the basis wave functions, which are described below. The model includes the sp-conduction band, d electrons, metal core states, and metal plasmons. For the W(110), the full set of $5s$, $5p$, $5d$, $6s$, and $6p$ states is included. The $5s$, $5p$, and $5d$ electrons are explicitly introduced by means of localized wave functions, which have been calculated by including relativistic effects[21] and are centered at the lattice sites. The valence sp electrons are described in an effective one-electron model. The wave functions are taken as eigenfunctions of the Sommerfeld model and have been orthogonalized to the core states of the metal atoms. On the W-tip atom, the $5d$-$6s$-, and $6p$-wave functions are taken into account.[22,35] On the Al-tip atom, the $3s$ and $3p$ valence orbitals are accounted for. They are described by a basis set of *ab initio* wave functions found in the literature.[23] An accurate treatment of wave function tails in the barrier is essential for any theory of tunneling. The basis wave functions chosen here have the correct asymptotic behavior in the barrier and artifacts, which might occur with calculations based on Gaussian or plane-wave basis sets, are absent.

The description of the metal surfaces requires input values, which are taken from experiment and band-structure calculations available in the literature: the work function, the inner potential depth, the energetic position, and the width of the sp-d hybridization gap, the lattice constants, and the energetic position of the d band.[20–24] Of some relevance for the tunnel current is the sp-d hybridization gap for W(110), which was extracted from relativistic band-structure calculations.[24] It extends from the Fermi level down to -2.22 eV below E_F. This means that for a small applied bias with a W-tip base, electrons will tunnel only into the W d band and not into the W $6sp$ band.

C. Method of solution: Calculation of total energy and forces

The Hamiltonian is solved in a self-consistent spin-unrestricted screened Hartree-Fock approximation, in order to evaluate the electronic structure, the interaction forces, and the tunnel current. This is an approximation to dynamic Hartree-Fock, which would yield the exact solution of the problem. The dynamic Hartree-Fock procedure is formally similar to the standard unrestricted Hartree-Fock formalism with the important difference that the effective potential seen by the electrons becomes energy dependent, because the Coulomb repulsion of the electrons is described by a nonlocal, energy-dependent self-energy $\Sigma(\mathbf{r},\mathbf{r}';E)$. The equation replacing the Fock equation in dynamic Hartree-Fock is sometimes called the Dyson equation and the eigenstates Dyson orbitals [cf. Eq. (8) below]. Another common name is the quasiparticle equation and quasiparticle states. Different names for the dynamic Hartree-Fock theory are Green-function theory or many-body field theory.

In the dynamic Hartree-Fock procedure, the Fock equations have, in principle, to be solved for any value of the energy parameter E in the self-energy and for any such value, one obtains a set of ''orbital energies'' $E_n(E)$. The correct quasiparticle energies are those that satisfy the condition

$$E_n(E)=E. \tag{7}$$

All one-particle properties can be obtained from the quasiparticle energies $E_n(E)$ and the corresponding one-particle wave functions $\psi_n(\mathbf{r};E)$. The Fock equation in the dynamic Hartree-Fock procedure reads

$$H_1\psi_n(\mathbf{r};E)+\int \mathbf{d}^3\mathbf{r}\Sigma(\mathbf{r},\mathbf{r}';E)\psi_n(\mathbf{r};E)=E_n(E)\psi_n(\mathbf{r};E). \tag{8}$$

H_1 contains the kinetic energy and the potential energy due to the ion cores. Electron-electron repulsion and screening are accounted for by the self-energy $\Sigma(\mathbf{r},\mathbf{r}';E)$. The electron density is expressed as

$$\rho(\mathbf{r})=\sum_{E_n<E_F}\eta_n\psi_n^*(\mathbf{r};E_n)\psi_n(\mathbf{r};E_n). \tag{9}$$

The sum is over those poles $E_n=E_n(E=E_n)$ of the Green function $G(\mathbf{r},\mathbf{r}';E)$, with residues η_n, which lie below the Fermi level. The poles are the exact ionization levels ($E_n<E_F$) and affinity levels ($E_n>E_F$) of the N-electron system. The residues are the amplitudes of the lines in the single-particle excitation spectrum. The total energy is obtained by

$$E_0=\frac{1}{2}\sum_{E_n<E_F}\eta_n[E_n+H_1(n,n)]. \tag{10}$$

The forces are then calculated by directly evaluating the gradient of the total-energy surface.

LDA does not appear as a mathematically well-defined approximation to the quasiparticle equation. Hartree-Fock is very bad for solids, e.g., the density of states of a metal is zero at the Fermi level. The reason is that the self-energy contains the unscreened (i.e., infinitely long ranged) electron-electron repulsion. Therefore, we use the spin-unrestricted *screened* Hartree-Fock theory, which yields approximations to the exact quasiparticle energies and wave functions and avoids the above-mentioned deficiencies of the Hartree-Fock method. In this approximation, the residues η_n are either unity or zero. Correlation effects are accounted for by screening the Coulomb interaction via the polarization of the environment. In order to solve the problem on a computer, the discretization technique for the sp bands of the metal surfaces, described in Ref. 25, is applied.

D. Analysis of the tip-sample interaction

The analysis is in close analogy to the procedure proposed by Ruedenberg for the analysis of the gas phase chemical bond, which is the accepted way of interpreting chemical forces.[26] This interpretation is based on an expansion of the wave functions of the interacting system in terms of the eigenfunctions of the separated, noninteracting system. In this way, it is possible to get an idea of how the chemical compound is formed from its constituent parts.

The starting point for a physical interpretation of the tip-sample interaction is the population analysis. Populations are defined by projecting the quasiparticle one-electron wave functions $|\psi_n\rangle$ on either the input basis $|a\rangle$ or the dual (reciprocal) basis $|\hat{a}\rangle$. We define the one-electron density operator:

$$P=\sum_{E_n\leqslant E_F}|\psi_n\rangle\langle\psi_n|. \tag{11}$$

Forming the scalar product of the dual basis functions ($|\hat{a}\rangle=\Sigma_b S_{ab}^{-1}|b\rangle$ yields

$$\langle\hat{b}|\hat{a}\rangle=(S_{ba})^{-1}, \tag{12}$$

where S is the overlap matrix of the input basis functions. Hence, the net population can be written in the form

$$\langle\hat{a}|P|\hat{a}\rangle=\langle a|S^{-1}PS^{-1}|a\rangle=\langle a|\widetilde{P}|a\rangle. \tag{13}$$

The trace of the $\widetilde{P}$ matrix is not equal to an integral number of electrons. To achieve this, the density operator has to be evaluated in a mixed representation:

$$\langle a|P|\hat{a}\rangle=\langle a|PS^{-1}|a\rangle=\langle a|S\widetilde{P}|a\rangle. \tag{14}$$

The trace of $S\widetilde{P}$ equals N, the total number of electrons. One can, therefore, extract the quasiclassical charge $(S\widetilde{P})^{\mathrm{diag}}$ from the diagonal elements of the one-electron density operator $\widetilde{P}$. This leaves a rest, which together with the off-diagonal $\widetilde{P}$-matrix elements have the meaning of interference one-electron density:

$$\widetilde{P}=(S\widetilde{P})^{\mathrm{diag}}+\widetilde{P}^{\mathrm{intf}}. \tag{15}$$

The quasiclassical density satisfies the electron conservation rule. An analogous partitioning exists for the two-electron density operator and the total energy can be expressed using these density matrices.[26] Using the respective parts of the density operator, the components of the interaction energy between tip and sample surface can be defined as follows:

$$E_{\mathrm{el}}^{\mathrm{tot}}=E_{\mathrm{el}}^{\mathrm{qc}}+E^{\mathrm{intf}}, \tag{16}$$

$$E_{\mathrm{tot}}=E_{\mathrm{el}}^{\mathrm{qc}}+V_{\mathrm{core\text{-}core}}+E^{\mathrm{intf}},\quad E_{\mathrm{el}}^{\mathrm{tot}}=E_{\mathrm{el}}^{\mathrm{tot}}(\mathrm{LR})+E_{\mathrm{el}}^{\mathrm{tot}}(\mathrm{SR}),$$

$$E_{\mathrm{el}}^{\mathrm{qc}}=E_{\mathrm{el}}^{\mathrm{qc}}(\mathrm{LR})+E_{\mathrm{el}}^{\mathrm{qc}}(\mathrm{SR}),\quad E^{\mathrm{intf}}=E^{\mathrm{intf}}(\mathrm{LR})+E^{\mathrm{intf}}(\mathrm{SR}). \tag{17}$$

LR stands for ''long range,'' meaning image contribution and SR stands for ''short range,'' meaning local contributions.

E. The tunnel current

Although results for the tunnel current are presented, this is not a major issue of this paper. Therefore, we present only the final formula and postpone the derivation to a later publication[28] stressing, however, that the tunnel current is calculated *exactly* within the spin-unrestricted screened Hartree-Fock approximation. The tunnel current is given by[27]

$$\frac{\hbar J}{2\pi e}=\sum_{f,i}|\langle\mathbf{f}|\widetilde{V}_{\mathrm{tip\text{-}sample}}|\mathbf{i}+\rangle^2\delta(E_f-E_i). \tag{18}$$

$\langle\mathbf{f}|$ indicates a one-electron wave function of the sample electrode unperturbed by the tip (for bias positive voltage, when the tunneling is from the tip into the sample). It should be considered as the state in which the electron is prepared when a measurement of the current is performed. $|\mathbf{i}+\rangle$ is a quasiparticle function of the total Hamiltonian, including the interaction $\widetilde{V}_{\mathrm{tip\text{-}sample}}$ between the tip and the sample surface. $+$ and $-$ signs indicate incoming and outgoing scattering boundary conditions, respectively. E_f and E_i are the one-electron energies of the states involved. The exact form of $\widetilde{V}_{\mathrm{tip\text{-}sample}}$ is described in Ref. 28. The potential induced by the tip atom is described by a set of basis orbitals $\{|\mu\rangle\}$, which are localized in the region around the tip. This localized basis set consists of atomic orbitals describing the tip atom plus a set of tip projected metal states constructed from the continuum states. Decay operators describing the decay of discretized states into the continuum are introduced as

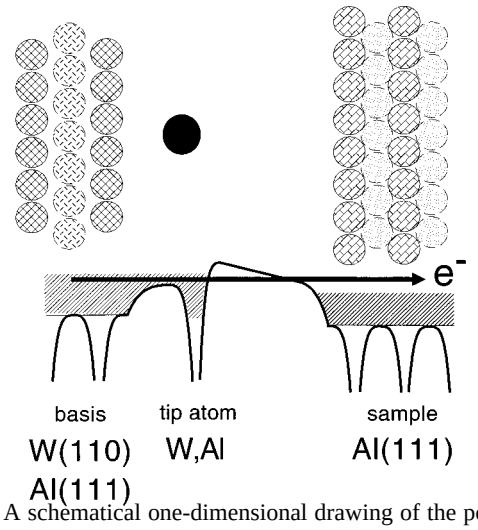

FIG. 3. A schematical one-dimensional drawing of the potential between the tip and the Al(111) surface in the neighborhood of the tip atom.

$$D^{\mathrm{ini}}(E) = -\frac{1}{\pi}\sum_i \frac{|\mathbf{i}\rangle\langle\mathbf{i}|}{E-E_i}, \tag{19}$$

$$D^{\mathrm{fin}}(E) = -\frac{1}{\pi}\sum_f \frac{|\mathbf{f}\rangle\langle\mathbf{f}|}{E-E_f}, \tag{20}$$

with matrix elements in the dual representation:

$$\widetilde{D}^{\mathrm{ini}}_{\mu\nu}(E) = -\frac{1}{\pi}\sum_{\lambda\kappa} S^{-1}_{\mu\lambda}\sum_i \frac{\langle\lambda|\mathbf{i}\rangle\langle\mathbf{i}|\kappa\rangle}{E-E_i} S^{-1}_{\kappa\nu}, \tag{21}$$

where $\{|\mu\rangle\}$ denotes the localized basis described above, $\{|i\rangle\}$ are the asymptotic continuum states describing the incoming electron, $\{|f\rangle\}$ are the asymptotic continuum states describing the outgoing electrons in the sample. The tunneling current has the form

$$\frac{\hbar J}{2\pi e} = \int_{E_1}^{E_2} dE\ \mathrm{Tr}\langle\mu|\widetilde{T}^{-}(E)|\nu\rangle\langle\nu|\mathrm{Im}\widetilde{D}^{\mathrm{fin}}(E)|\lambda\rangle \tag{22}$$

$$\langle\lambda|\widetilde{T}^{+}(E)|\kappa\rangle\langle\kappa|\mathrm{Im}\widetilde{D}^{\mathrm{ini}}(E)|\mu\rangle. \tag{23}$$

A notation is used where $|\nu\rangle\langle\nu|$ implies summation over all states $|\nu\rangle$ and Tr denotes summation over the states $|\mu\rangle$. $\langle\mu|\widetilde{T}^{\pm}(E)|\nu\rangle$ is a matrix element of the transition operator.

III. DESCRIPTION OF THREE INVESTIGATED TIPS

A first step in the theoretical investigation is to study the electronic properties of isolated tips. The chemisorption theory described in the previous section has been applied to study metal tips consisting of a single atom (W, Al) adsorbed on a metal surface. An ideal STM tip will be one atom adsorbed on a group of other metal atoms, which is embedded in an infinitely extended metal electrode. For a first theoretical attempt, we will model this as a single atom adsorbed on a flat W(110) or Al(111) surface (cf. Fig. 3). Results for a cluster tip will be presented elsewhere.

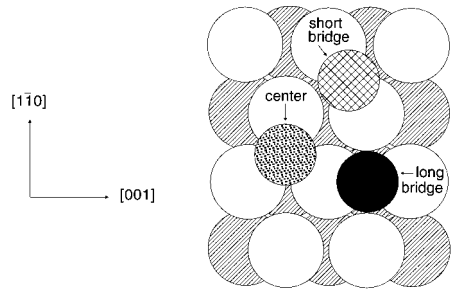

FIG. 4. Sites for self-adsorption and for Al atom adsorption on W(110).

A. W/W(110)

The first tip studied consists of a W atom adsorbed on a W(110) surface. The possible adsorption sites are displayed in Fig. 4. The adsorption site of lowest energy was found to be in the long bridge. Figure 5 shows the potential-energy curve for a W atom above the bridge position on W(110) versus the perpendicular distance. The adsorption energy at the equilibrium position equals 5.3 eV. The diffusion barrier via the tip position is found to be 0.8 eV. These findings agree nicely with experimental data obtained with field-emission microscopy.[29] The electronic structure of the adsorbed W atom representing the apex of the tip has a decisive influence on the tunnel current. An important quantity in this respect is the modification of the local density of states, due to the presence of the tip atom, or, more precisely, the spectral resolution of the W-tip-atom orbitals $\{|A\rangle\}$ in the eigenstates $\{|\psi_i\rangle\}$ of the tip Hamiltonian H^{tip}:

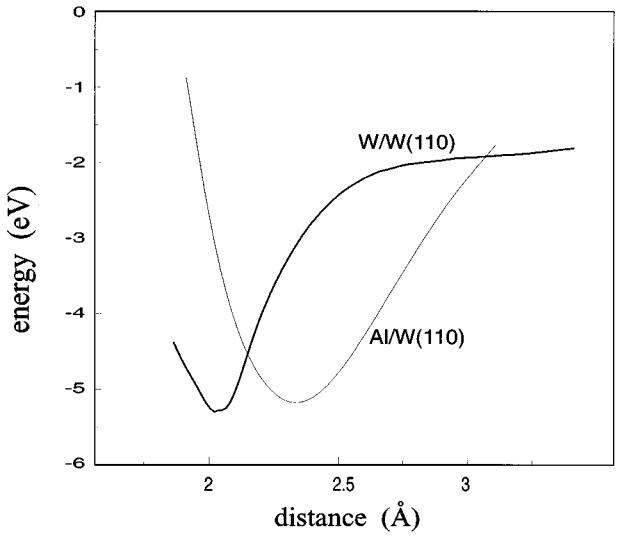

FIG. 5. Potential-energy curves for W and Al on W(110) versus perpendicular distance. The distance is with respect to the first layer of metal atoms. The equilibrium distance of the W-tip atom with respect to the W(110) surface is 2.09 Å in the long bridge site. The equilibrium distance of the Al-tip atom, with respect to the W(110) surface is 2.38 Å in the long bridge position.

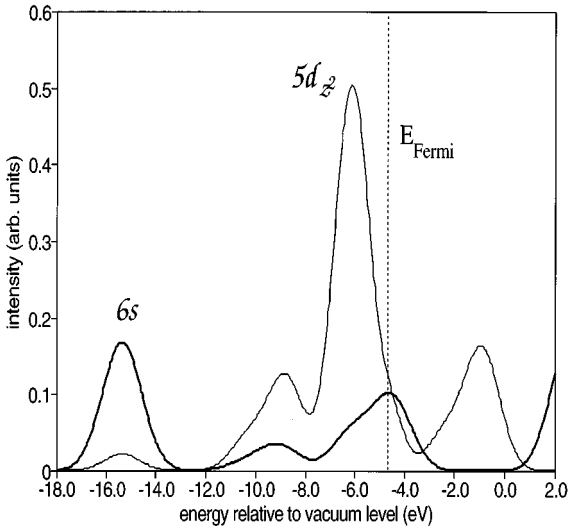

FIG. 6. Spectral resolution of the W 5_{dz^2} and $6s$ tip orbitals (majority spin) for an isolated W tip at the equilibrium adsorption distance of the W atom.

$$\rho_A(E)=\sum_i |\langle A|\psi_i\rangle|^2\delta(E-E_i). \tag{24}$$

An isolated W atom has four electrons in the $5d$ shell and two electrons in the $6s$ orbitals, all deeper shells being completely filled. In Fig. 6, we show the spectral resolution of the $5d_{z^2}$- and $6s$-tip orbitals (majority spin). The tunnel current will depend on the weight of these spectral functions at the Fermi level. Due to the bonding-antibonding character of the spectral functions, the weight near the Fermi level will vary with the distance of the tip atom from the base and with any modification of the surrounding electron density.

An understanding of the interaction forces between tip and sample requires also an insight into the bonding mechanism of the tip atom on its base metal. We perform the analysis described in Sec. II D. The analysis partitions the energy components into quasiclassical and interference contributions. In Table I, these energy components of the binding energy of W on W(110) are further subdivided into contributions arising from the image interaction and the local interaction.

The components listed in the row ''frozen local charge'' correspond to the situation where the charge on the tip atom and in the adjacent environment in the metal (this is the ''local region'') has been frozen as it is on the noninteracting tip atom plus tip base system. The column ''image'' contains the energy contribution, due to the polarization of the metal electrons outside the local region in response to the potential induced by the tip atom. The gain in image energy of -34.63 eV for the frozen charge configuration is mainly due to reduction of electron-electron repulsion in the local region arising, because each electron experiences an attraction by the images of the other electrons. The sum of the contributions for the frozen local charge situation is still considerably repulsive.

The quasiclassical charge redistribution may be visualized as a fractional occupation of the eigenstates of the separated system. It contains that part of the charge rearrangement, which is not due to mixing of wave functions. The second row of Table I lists the differences between the quasiclassical energies $V_{\text{core-core}}+E_{\text{el}}^{\text{qc}}(\text{SR})$ and $E_{\text{el}}^{\text{qc}}(\text{LR})$ and the corresponding contributions from the frozen local charge. In gas phase chemistry, the quasiclassical contribution to the interaction energy is usually interpreted as a preparation (''promotion'') for optimal interference, i.e., for a mixing of wave functions that leads to a maximum gain in energy. This interpretation is also applicable for the present case, where the adsorptive interaction is stable due to the interference contribution $E^{\text{intf}}(\text{SR})$ and $E^{\text{intf}}(\text{LR})$ listed in the third row of Table I. It is, however, important to note that the local complex on its own would not be stable just because of the energy lowering due to interference in the local region. The image interaction, i.e., the polarization of the remaining part of the tip base metal, is essential for preparing the ground for a local chemical bond. Somewhat contrary to the intuitive feeling, the image interaction leads to energy lowering, not only in the case when the net charge on the adparticle is nonzero. In fact, in the present case, we have essentially a neutral W-tip atom that is bonded to the adjacent atoms in a covalent way.

TABLE I. Energy components (in eV) of the interaction of a W-tip atom with the W(110) base at the equilibrium distance of 2.09 Å .

	Local	Image	Total
Frozen local charge	54.73	−34.63	20.10
Quasiclassical change	17.42	−3.74	13.68
Interference energy	−31.86	−7.26	−39.06
Sum	40.29	−45.57	−5.28

B. Al/W(110)

Figure 5 contains also the potential-energy curve for an Al atom on W(110) in the long bridge position. Here, no experimental or theoretical data are available for comparison. An Al atom behaves chemically quite differently from a W atom. Al has an ionization energy of 5.986 eV, which is not much larger than that of a Li atom (5.39 eV; ionization energy of W: 7.98 eV). The work function of W(110) is 5.219 eV. This implies that already at 4.7 Å from the image plane ($\approx$6 Å from the geometrical surface), the image shift would be large enough to ionize the Al $3p_z$ orbital. Taking into account the broadening of the $3p_z$ level due to the interaction with the continuum, we understand that already at distances where overlap effects are small, the $3p_z$ orbital becomes partially depleted of electron charge, and this gives rise to a classical image force. Therefore, at separations much larger than the equilibrium adsorption distance, where for W on W(110) no gain in energy is obtained, there is already a lowering of the energy for Al on W(110), and the potential energy of this system lowers in a rather soft way. This behavior differs from the way the potential for a W atom varies in front of the W(110) surface, because the image shift is not large enough in this case and the W atom will not be partially ionized. The image energy of the positively polarized aluminum atom is the dominating contribution to the energy lowering in the long-range part of the attractive Al/W(110) potential.

TABLE II. Energy components (in eV) of the interaction of an Al-tip atom with the W(110) base at the equilibrium distance of 2.38 Å .

	Local	Image	Total
Frozen local charge	16.94	−9.61	7.33
Quasiclassical change	−10.70	1.42	−9.28
Interference energy	−0.95	−2.28	−3.23
Sum	5.29	−10.47	−5.18

Near the equilibrium distance, however, chemical forces of stronger character dominate, although we know that the image interaction in its general sense will have a significant influence on the nature of the chemisorption bond. The partitioning of the binding energy of Al/W(110) at the equilibrium distance is displayed in Table II. The frozen asymptotic charges on Al and the W(110) surface repel each other similar to the W/W(110) system. The quasiclassical charge redistribution in Al/W(110), however, leads to energy lowering contrary to the W/W(110) system. This gain in quasiclassical energy has little to do with the positive polarization of the adsorbing Al atom. It is rather connected with the capability of the electrons on the tip atom to screen its positive charge. If the screening in the local region is not efficient, the system can gain more energy by pushing the electrons on the tip atom somewhat aside and letting the metal electrons profit from the attraction by the tip ion. This formulation has, of course, to be understood in the Ruedenberg sense and does not mean violation of the fundamental principle that electrons are indistinguishable. The energy profit by the metal electrons can already be achieved to a large part via fractional reoccupation of the eigenfunctions of the separated partners and hence it appears as a large gain in the quasiclassical energy. We realize that this quasiclassical reorganization of charge is connected with a loss in the image energy, which means that the image interaction is not the main driving force for bond formation at this separation, although the image reduction of the electron-electron repulsion is an indispendsable condition to activate this mechanism. Because the system tries to gain energy in a quasiclassical way, the gain in interference energy is rather small. The gain in quasiclassical energy is not typical of a normal gas phase covalent chemical bond. In fact, it appears that this type of bonding is special for adsorption at metal surfaces and it should not be misinterpreted as an ionic bond. This kind of bonding has also been observed for nonmetallic adsorbates like hydrogen atoms, for example.[17]

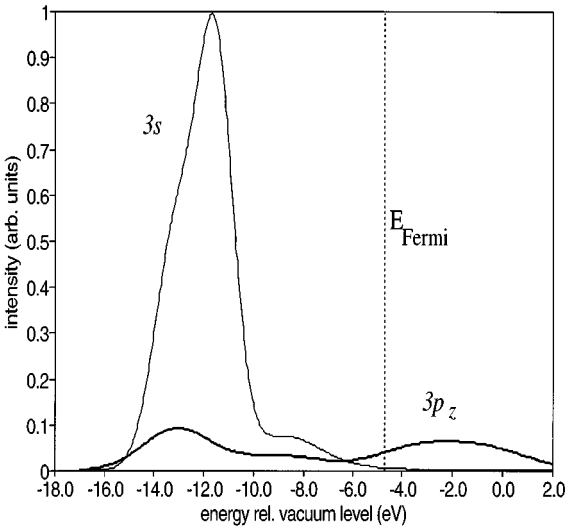

FIG. 7. Spectral resolution of the Al $3p_z$ and $3s$ tip orbitals for an isolated Al/W(110) tip at the equilibrium position of the Al atom.

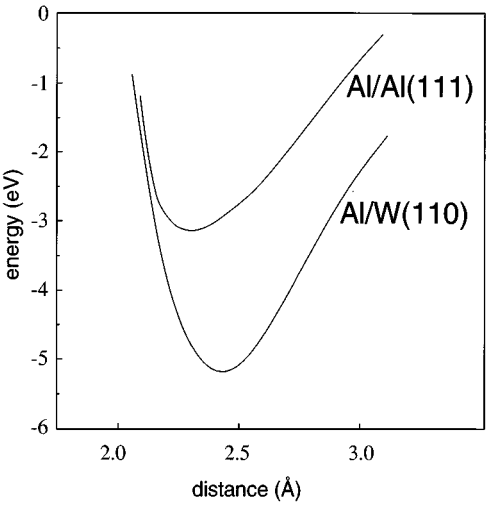

FIG. 8. Potential-energy curve for Al on Al(111) vs distance measured with respect to the first layer of aluminum atoms.

The spectral distributions for this tip [cf. Eq. (24)] are displayed in Fig. 7 and show considerably less spectral weight at the Fermi level than the tungsten tip. This suggests that the Al/W(110) tip might result in higher tunnel resistance. Compared to Fig. 6, we see that the smaller spectral weight of the tip orbitals at the Fermi energy can be traced back to the lack of *d* states on the Al atom.

C. Al/Al(111)

For a pure Al tip, the potential-energy curve is displayed in Fig. 8. Here, a comparison with first-principle calculations in the local-density approximation is possible and provided in Table III. The equilibrium distance is smaller in the calculations by Stumpf[30] and Feibelman,[31] because they allowed all surface atoms to relax, whereas they have been fixed at their bulk equilibrium positions in our theory.

The character of the Al/Al(111) bonding is quite similar to that of Al/W(110), but as we observe from the data in

TABLE III. Bond distance and adsorption energy for Al self-adsorption on Al(111).

	Equilibrium distance	Adsorption energy	
	(Å)	(eV)	Ref.
Al(111)	2.1	2.7	31
Al(111)	2.1	3.2	30
Al(111)	2.3	3.1	this work

TABLE IV. Differences of energy components (in eV) between Al/W(110) and Al/Al(111) at their respective equilibrium distances.

	Local	Image	Total
Frozen local charge	−1.74	1.38	−0.36
Quasiclassical change	−3.71	−0.51	−4.22
Interference energy	1.95	0.58	2.53
Sum	−3.50	1.45	−2.05

Tables II and III, it is more than 2 eV weaker on Al(111). This is important, if we want to consider material transport from an aluminum surface to a tungsten tip. To understand the origin of this energy difference we present in Table IV the difference in energy component for Al/W(110) and Al/Al(111). The equilibrium distance of the Al atom is further away on the W(110) surface. Therefore, the electrostatic repulsion for the frozen local charge configuration is less repulsive. This is nearly compensated by the smaller image polarization, due to the larger distance, so that the local frozen charge configurations differ only slightly for the two tips. The largest variation between Al/Al(111) and Al/W(110) appears in the local quasiclassical energy gain, which is roughly 3.71 eV more attractive for Al on W(110). The reason for this is that the W(110) surface has large occupied and empty *d* density of states around the Fermi level, which means that the *d* electrons are rather polarizable. In addition, the *d* orbitals have a geometrically favorable shape to yield a large overlap in the region of the Al core. The additional quasiclassical gain for Al/W(110) is partially compensated by a less attractive interference. A closer inspection reveals that for the W(110) surface interference is more attractive in the metal and more repulsive in the region between the tip atom and the metal surface. Interference implies orthogonalization of the one-electron wave functions, which is necessary to obey the Pauli exclusion principle. If the interference cannot be exploited to gain energy, it will usually become repulsive in regions of large overlap, because it just serves for orthogonalization. The other differences are rather minor. We summarize the comparative energy analysis of the Al-terminated tips by remarking that (1) the potential-energy curves are soft on both surfaces, (2) energy is gained by a quasiclassical charge redistribution in the metal in order to profit from the attraction by the tip core, (3) the attraction is larger on W(110), because of the presence of *d* states.

The spectral distribution of the 3*s* tip orbital for this tip is displayed in Fig. 9. It shows even less structure than for Al/W(110).

In this paper, we do not present results for the elastic relaxation of the metal atoms in the close vicinity of the tip atom. They are fixed at the equilibrium lattice sites typical for the ideal crystal.

IV. THE W(110)/W TIP IN INTERACTION WITH AN Al(111) SAMPLE SURFACE

The case of an atom in interaction with two plane electrodes is handled in a similar fashion as described above. The wave functions for the W surface together with its adsorbed tip atom are just those of the one-atom chemisorption problem. Multiple image effects arising from the polarization of one electrode by the induced charge density in the other electrode are included. The effect of the distortion by the electric field resulting from the different work functions on the electronic structure of the tip atom is included. A schematical one-dimensional drawing of the one-electron potential in the region of the tunnel tip is shown in Fig. 3.

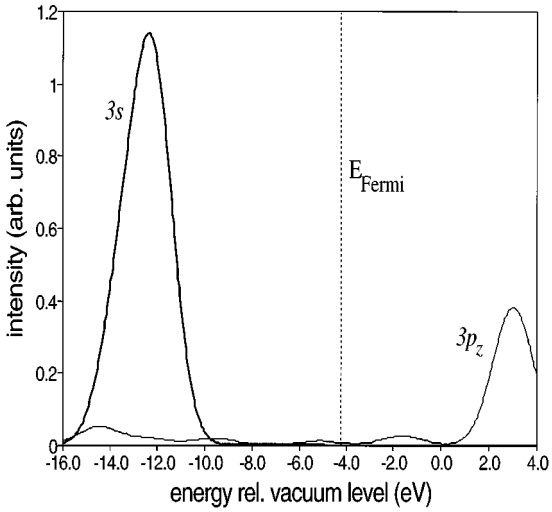

FIG. 9. Spectral resolution of the Al $3p_z$ and $3s$ tip orbitals in the energy band of Al(111) at the equilibrium adsorption distance of the Al atom.

Figure 10 shows the calculated tip-sample interaction energy and the interaction force gradient as a function of tip-sample separation. The asterisk markers indicate the experimental results of Dürig and Züger for an Ir tip on an Al foil.[16] The tip-sample distance is not known in experiment, so the experimental data have been adjusted in such a way that the points of zero force gradient coincide.

The experimental force gradient is one order of magnitude smaller than the calculated one. Figure 11 compares the dis-

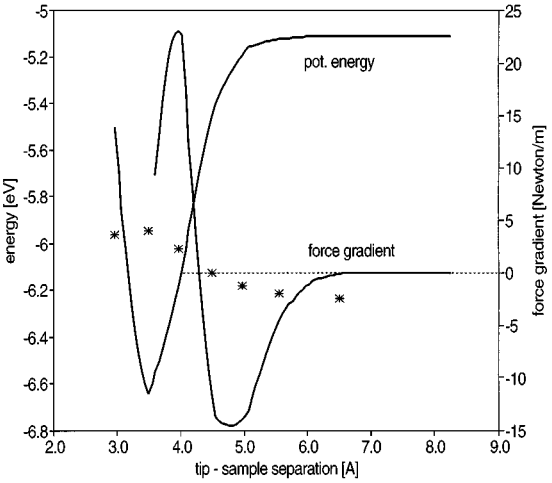

FIG. 10. Interaction energy and force gradient of a tungsten tip with an Al(111) surface. The tip is positioned above an Al atom. The experimental data for the force gradient of an Ir tip on an Al foil (∗) have been taken from the work of Dürig and Züger (Ref. 16).

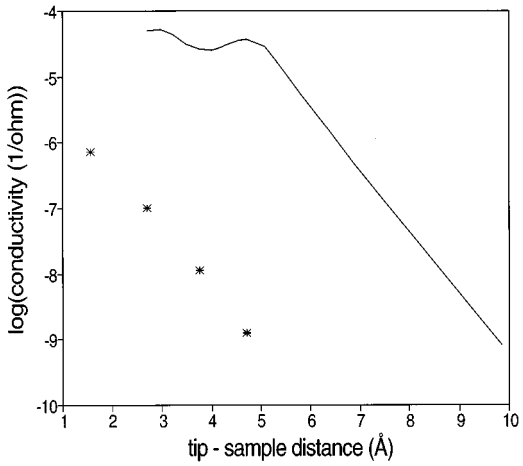

FIG. 11. Conductivity ($\log_{10}$) of the W(110)/W-Al(111) system vs tip-sample distance (in Å). The experimental data of Dürig and Züger from Ref. 16 using an Ir tip on an Al foil are displayed for comparison with asterisks.

tance dependence of the calculated and the measured tunnel conductivity. With the above adjustment of the tip relative to the sample surface, the experimental values of the tunnel conductivity are three to four orders of magnitude smaller than the theoretical ones. In addition, the data points from the experiment would, with the above adjustment, correspond to unphysically short distances. Obviously the tungsten model tip cannot describe the experiments by Dürig and Züger.[16]

V. THE W(110)/AL TIP IN INTERACTION WITH AN AL(111) SAMPLE SURFACE

The hint to the origin of the above-mentioned discrepancy between theory and experiment comes already from the experimental side. It has been suggested several times that during the process of tip preparation, material transport from the Al sample to the tip might occur.

A. Potential-energy surface: The transfer of an adsorbed Al atom from Al(111) towards W(110)

We investigated this point by calculating the potential-energy surface for the perpendicular motion of an Al atom between a W(110) electrode and an Al(111) electrode for zero applied bias. Figures 12(a) and 12(b) give two different graphical representations. In the gray scale representation of the potential-energy surface [Fig. 12(b)], dark regions correspond to low (attractive) energy and bright regions to higher (more repulsive) energies. At the right-hand side of the figure, we have the situation of an Al atom adsorbed on Al(111) facing the W electrode at large distances. The two white cutting lines indicate the directions along which the potential varies, if the Al-tip atom is moved perpendicular to the electrodes for *fixed* electrode separation. For large electrode separations (white line further to the right), there is an activation barrier for the movement of the Al atom between the two minima corresponding to equilibrium adsorption on the two electrodes. For shorter electrode separations (closer than 6 Å , white line further to the left), the activation barrier

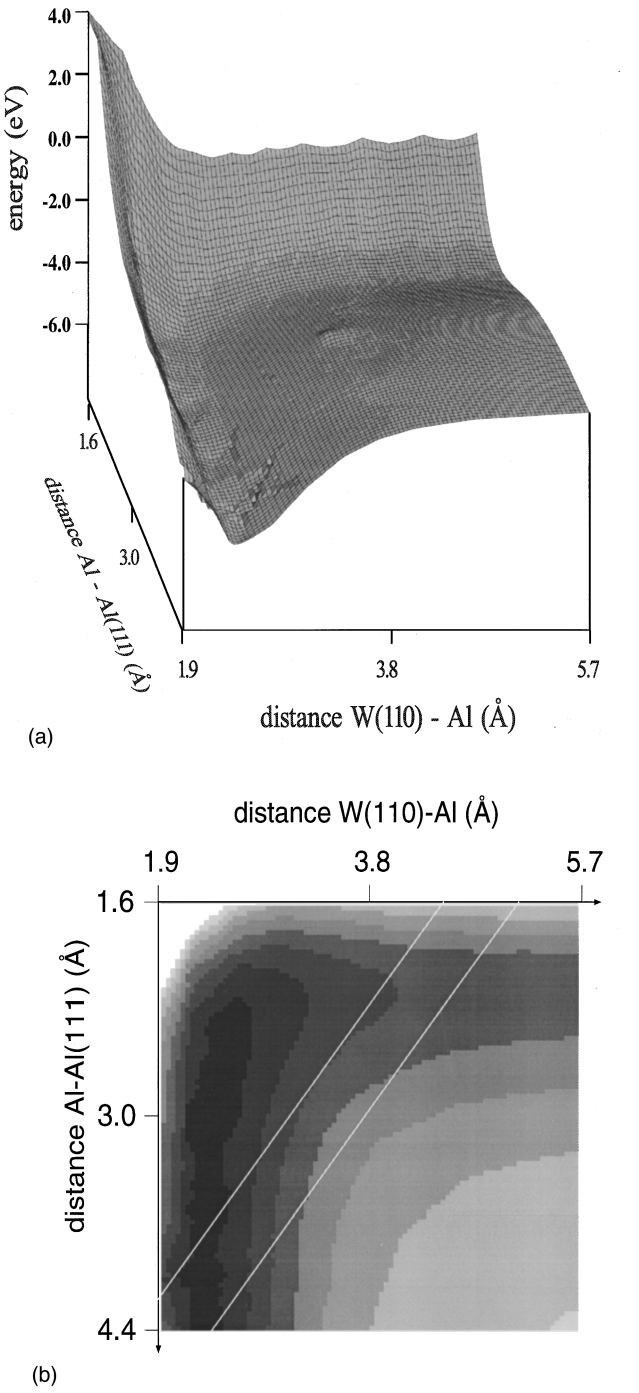

FIG. 12. (a) Potential-energy surface for W(110)-Al-Al(111). (b) Gray scale representation of the potential-energy surface for W(110)-Al-Al(111).

vanishes and the potential energy of the Al atom decreases monotonously on its way from the Al electrode to the W electrode. This means that for close approach of the W electrode to the Al sample, an Al atom adsorbed on the Al(111) surface experiences a force that pulls it towards the W electrode. The physical reason for the vanishing of the activation barrier at close electrode separation is rather obvious from the above analysis of the adsorption energy of an Al-tip atom on the two electrodes. The softness of the adsorption curves

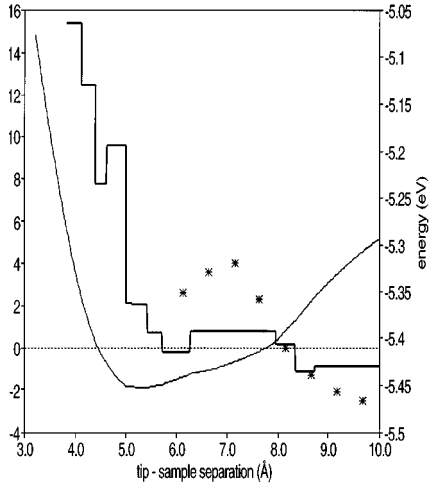

FIG. 13. Potential-energy curve and force gradient (steplike curve) for a W(110)/Al tip above an Al(111) surface. The experimental data of Dürig and Züger (Ref. 16) for the force gradient of an Ir tip on an Al foil are indicated with asterisks.

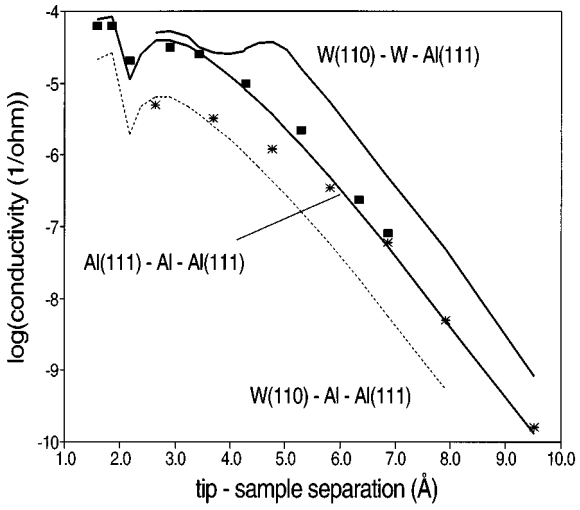

FIG. 14. Theoretical conductivity ($\log_{10}$) versus distance curves for three different tips in comparison with experimental data for Ir/Ag (black rectangles—from Ref. 33) and Ir/Al (asterisk—from Ref. 16).

and the quasiclassical character of the chemisorption bond lead to the continuous decrease of the energy between the two electrodes.

B. Tunnel current and force gradient

Figure 13 shows the interaction energy and the force gradient for an Al/W(110) tip above an Al(111) surface. The Al atom has been kept fixed at its adsorption equilibrium distance, with respect to the W(110) surface. The asterisks indicate the force gradient values for an Ir tip above an Al foil as measured by Dürig and Züger.[16] In these experiments, the point of contact was not reached, which would have been a convenient method for calibrating distances in experiment against the theoretical ones. We, therefore, identify the zero of the force gradient in the experimental curve with the first theoretical zero at largest distance.

In the mentioned experiments, the force gradient between tip and sample was measured simultaneously with the tunnel current for small applied bias (0.1–0.3 V). In the theory and in the experiment, the measured force gradient is slightly attractive at further distances and turns repulsive several angstroms before the plateau in the conductivity is reached. Only at smaller distances (where the measurements became unstable) does the force become strongly repulsive. The exact tunnel conductivity is calculated within the scattering theoretical approach, which has been outlined in Sec. II E. In Fig. 14, the theoretical conductivity-versus-distance curves in the limit of zero bias are plotted for the three investigated tips and compared with experimental data for an Ir tip above an Ag foil (black rectangulars)[33] and an Al foil (asterisks).[16] In the experimental data for the Ag foil, the scale for the tip-sample separation has been shifted, so that the steps in the conductivity-versus-distance curves agree in theory and experiment. (The physics of this step will be discussed elsewhere.) For the Al foil, the adjustment is based on the zero of the force gradient as outlined above. As it was remarked in connection with the spectral resolution of the tip orbitals in the base metal band, the Al/Al(111) tip yields smaller conductivity values than the tip with a W atom at the apex. Al/W(110) yields even smaller current, because of tunneling in the tungsten *d* band only. With the Al/W(110) tip, a satisfactory agreement between theory and experiment is achieved for both the force gradient and the tunnel current (cf. Figs. 13 and 14). The theory is even capable of reproducing the somewhat unexpected repulsive force gradient for tunnel currents corresponding to normal STM imaging conditions (cf. Fig. 13). For STM experiments on transition-metal surfaces, a repulsive force gradient has never been measured up to very short distances where stable operation of the STM becomes impossible. The theory explains these findings by material transport from an Al surface to the transition-metal tip and the special properties of the tip obtained in this way.

C. The special properties of the Al/W(110) tip

We now describe the physics behind these special properties of the Al/W(110) tip by comparing it with a tungsten tip. We make use of the formalism developed to analyze, in a quantitative way, the nature of the tip-sample interaction. This analysis is performed within the same procedure as it was used for the analysis of the adsorption bond of the tip atoms on the base metal surfaces.

In Table V, we compare the contributions to the tip-sample interaction energy of the W/W(110) and the Al/W(110) tips with the Al(111) surface with the Ruedenberg analysis of the chemical bond in H_2 and the HeH^+ ion. ''Frozen local charge'' refers now to the superposition of the charge distributions of the tip base with its adsorbed metal atom and that of the sample surface when they do not perturb each other. Qualitatively, we have the same characteristics as discussed above for the adsorption of a W and an Al atom, i.e., the tungsten tip makes a gas-phase-like interference bond with the Al sample, whereas the Al/W(110) tip gains energy quasiclassically. An important difference is, however, that for the Al/W(110) tip, the energy due to interference

TABLE V. Analysis of tip-sample interaction in comparison to the H_2 and HeH^+ molecule (energies in eV).

	W/W(110)-tip on Al(111) 4.81 Å	H_2	HeH^+	Al/W(110)-tip on Al(111) 3.23 Å
Frozen local charge	0.08	−0.3	0.2	0.86
Quasiclassical change	1.18	2.3	5.3	−2.19
Interference	−1.49	−6.0	−7.4	1.67
Sum	−0.23	−4.0	−1.9	0.34

with the sample wave functions is now repulsive. Together with the partially charged character of the Al-tip atom, this is the key point for understanding the behavior of this tip. From Table VI, we learn that the repulsive interference arises from the local interaction and a closer inspection shows indeed that it occurs in the region between the tip and the sample.

The zero of the force gradient at typical tunneling distances means just that the curvature of the potential-energy curve has changed its sign here. For large distances, the interaction between the Al/W(110) tip and the Al(111) sample is dominated by the multiple image effects, due to the charge on the Al-tip atom. This part of the potential-energy curve has a negative curvature (cf. Fig. 13). The multiple image force saturates at approximately 8-Å separation of the tip and the sample, because it merges into a general exchange-correlation potential. From that distance on, additional energy is gained by the quasiclassical dominated tip-metal interaction discussed above for the example of Al adsorption on W(110). Because of the repulsive interference energy, from this distance on, the energy decreases more slowly upon decreasing the tip-sample separation, compared to the distance range where the interaction was dominated by the image interaction. This implies, of course, a change in the curvature of the potential-energy curve and therefore the force gradient changes sign from negative at larger z to positive values at smaller interelectrode distances.

For the W tip, the situation is quite different as detailed in Table VII. The W-tip atom does not carry a charge and therefore the long-range attractive part due to multiple image interactions is absent in the tip-sample interaction curve (cf. Fig. 10). In Table VII we see that the quasiclassical charge rearrangement increases the local energy, but decreases the image energy. From this we conclude that the tip-sample interaction involves a quasiclassical charge redistribution on the W-tip atom, such that a hybridization of $6s$-, $6p_z$-, and $5d_{z^2}$-tip orbitals in the direction to the sample surface occurs. This acts as a preparation for forming a covalent chemical bond with the sample, which sets in more abruptly at smaller separations. Therefore, the curvature is larger in magnitude, but only at much smaller separations (cf. Fig. 10). We suggest this as the explanation for the experimental finding that when a transition-metal tip approaches a transition-metal sample (the atom at the apex of the tip has to be a transition-metal atom) the force gradient is much larger and always negative and the regime of positive force gradient is never reached.

VI. THE AL(111)/AL TIP IN INTERACTION WITH AN Al(111) SAMPLE SURFACE

From the way the tip is prepared in the STM experiments (i.e., pushing the tip into the sample surface and applying a voltage pulse), it is not clear that one would necessarily end up with a single Al atom on a W base. It might appear indeed more likely that a cluster of several Al atoms is transferred to the tip. This situation is perhaps theoretically better simulated by a pure Al tip. For this purpose, the interaction of a tip consisting of a single Al atom adsorbed on an Al(111) surface with an Al(111) sample surface was investigated as well.

This STM model has also been investigated by Ciraci, Baratoff, and Batra[34] in a supercell arrangement based on the local-density approximation. This theory, however, did not permit the calculation of the tunnel current. They calculated the total electronic charge density of the interacting tip-sample system and the force acting on the Al-tip atom. This force is, of course, different from the force acting between the sample and the tip as a whole, which is measured in experiment. In order to make contact with this theoretical effort, the force on the Al-tip atom was also evaluated in the present model Hamiltonian approach. Figure 15 shows the calculated potential-energy curve of the tip-sample interaction together with the force resulting from this curve. It also displays the force acting on the tip atom as evaluated in the two mentioned approaches. The force acting on the tip atom is, at least at small separations, much smaller than that be-

TABLE VI. Contributions to the interaction energy in eV for W(110)/Al-Al(111) at distance=3.23 Å.

	Local	Image	Total
Frozen local charge	2.12	−1.26	0.86
Quasiclassical change	−2.79	0.60	−2.19
Interference	2.10	−0.43	1.67
Sum	1.43	−1.09	0.34

TABLE VII. Contributions to the interaction energy in eV for W(110)/W-Al(111) at tip-sample separation of 4.81 Å .

	Local	Image	Total
Frozen local charge	0.20	−0.12	0.08
Quasiclassical change	2.18	−1.00	1.18
Interference	−1.22	−0.27	−1.49
Sum	1.16	−1.39	−0.23

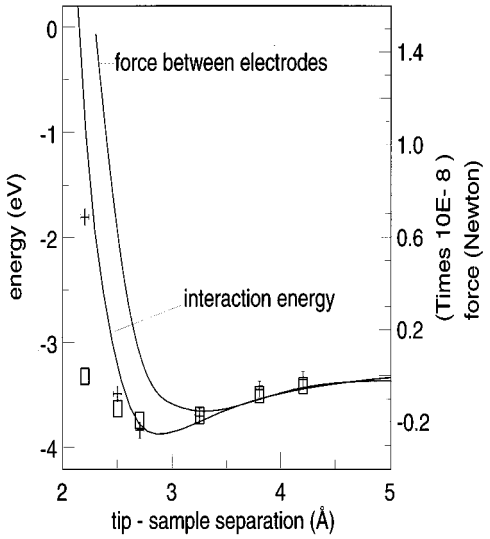

FIG. 15. The interaction energy between an Al/Al(111) tip and an Al(111) sample, the force between the two electrodes and the force acting on the Al-tip atom between the two electrodes (crosses). The force on the Al-tip atom calculated by Ciraci, Baratoff, and Batra (Ref. 34) for the same model in a supercell calculation is plotted with rectangles.

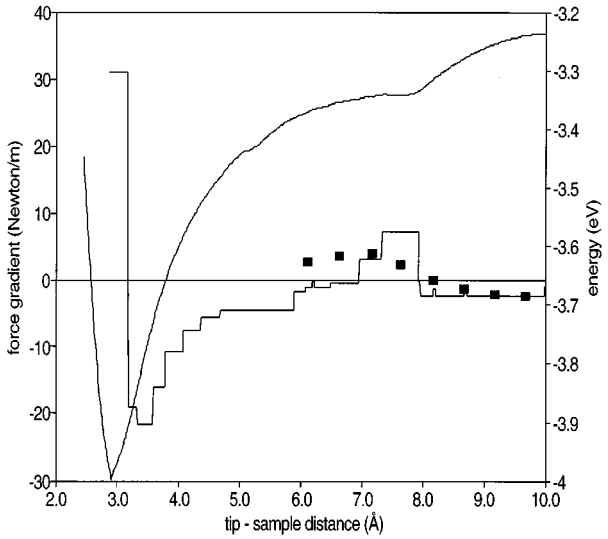

FIG. 16. Interaction energy and force gradient (steplike curve) for an Al/Al(111) tip above Al(111) surface.

tween tip and sample, because the total energy changes less when only one atom is moved instead of the whole tip. The comparison of this quantity as calculated within the two theories is favorable.

The main interest is, however, in the measurable force gradient between tip and sample at larger distances than displayed in Fig. 15. This is shown in Fig. 16, in comparison to the experimental data by Dürig and Züger.[16] The experimental distance (which can only be measured relative to an arbitrarily defined reference distance) has been adjusted again so that the zeros of the force gradients agree. At these large separations the behavior and the physics are quite similar to those of the Al/W(110) tip (cf. Sec. IV). At closer distances the behavior is, however, quite different. The interaction energy is significantly more attractive than for the Al/W(110) tip and this leads to a second pronounced minimum in the force gradient.

In this paper, we only studied the force gradient for a fixed tip atom-tip base distance. Of course, the tip atom will adjust its position according to the forces acting on it. Calculations taking this into account have been performed and lead to a relaxation of the tip-atom position of up to 0.5 Å (Ref. 35). This does not lead to any change of the physical picture presented here. One should, however, remark that with this relaxation taken into account the force on the tip atom (cf. Fig. 15) will always be zero and, therefore, this quantity has no meaning at all.

VII. CONCLUSIONS

The theory of the interaction of an Al atom with a W(110) and an Al(111) electrode has been presented within a spin-unrestricted screened Hartree-Fock method, which takes into account electron correlation, multiple image effects, and electric-field effects. The results favor a nonactivated spontaneous transfer of the Al atom from the Al surface to the W surface, even without an applied electric field, if the W(110) surface is brought close enough to the Al(111) electrode. The barrier for desorption from the Al(111) surface collapses and a directional driving force pulls the Al atom towards W(110). This behavior is due to the stronger chemisorption interaction of the Al atom with the tungsten surface. The reason is associated with the presence of the *d* electrons on tungsten, which can polarize towards the adatom, gaining energy from the attractive interaction with the Al core.

Our investigation suggests that Al atoms will be transferred to the tip in scanning tunneling microscopy, if an Al(111) surface is scanned with a tungsten tip. This will occur even in the limit of zero voltage at some critical electrode separation and has no relation to field-induced desorption. Of course, field effects might modify this behavior. However, our results demonstrate that no applied electric field is necessary for atom transfer beyond a critical electrode separation. Support that this is indeed what happens in experiment comes from the comparison of the tunnel current and force gradient variations with tip-sample distance. The calculated force gradient for the Al/W(110) tip above the Al(111) sample surface resembles closely the experimental results of Dürig and Züger[16] for an Ir tip on an Al film. The force between the tip and the sample reaches its attractive minimum at 8-Å tip-sample separation. At this separation, the slightly positively charged Al-tip atom is neutralized, due to the proximity of the sample electrode and the image interaction ceases to be of dominant importance. The theory explains the change in sign of the force gradient as a consequence of this change in the chemisorption interaction of the Al atom with the two metal surfaces. The comparison with the experimental force minimum might be used for an absolute calibration of the tip-sample distance.

The special properties of the tunnel tip, produced when an Al atom is transferred from the Al(111) sample to the W(110)-tip electrode, can yield an explanation of the experi-

mentally observed features with two different probing techniques, i.e., scanning tunneling and force microscopy. Using this tunnel tip, we reproduce the distance variation of both the tunnel conductivity and the force gradient, two seemingly unrelated quantities. This fact gives us confidence to claim that Al atom or cluster transfer indeed occurs when an aluminum surface is scanned by a tungsten tip even in the absence of an external electrical field.

[1] R. S. Becker, J. A. Geologic, and B. S. Swartzentruber, Nature **325**, 419 (1987); J. Foster, J. E. Frommer, and P. C. Arnett, *ibid*. **331**, 324 (1988); R. Emch, J. Nogami, M. M. Dovek, C. A. Lang, and C. F. Quate, J. Microsc. (Oxford) **152**, 129 (1988); Y. Z. Li, L. Vazquez, R. Piner, R. P. Andres, and R. Reifenberger, Appl. Phys. Lett. **54**, 1424 (1989); I.-W. Lyo and Ph. Avouris, J. Chem. Phys. **93**, 4479 (1990).

[2] H. M. Mamin, P. H. Guether, and D. Rugar, Phys. Rev. Lett. **65**, 2418 (1990).

[3] D. M. Eigler and E. K. Schweizer, Nature (London) **344**, 524 (1990).

[4] D. M. Eigler, C. P. Lutz, and W. E. Rudge, Nature (London) **352**, 600 (1993).

[5] I.-W. Lyo and Ph. Avouris, Science **253**, 173 (1991); Ph. Avouris and I.-W. Lyo, Appl. Surf. Sci. **60/61**, 426 (1992).

[6] H. J. Kreuzer, L. C. Wang, and N. D. Lang, Phys. Rev. B **45**, 12 050 (1992).

[7] N. D. Lang, Phys. Rev. B **45**, 13 599 (1992); **49**, 2067 (1994).

[8] R. E. Walkup, D. M. Newns, and Ph. Avouris, Phys. Rev. B **48**, 1858 (1993); J. Electron Spectrosc. Relat. Phenom. **64/65**, 525 (1993).

[9] S. Gao, M. Persson, and B. I. Lundqvist, Solid State Commun. **84**, 271 (1992); J. Electron Spectrosc. Relat. Phenom. **64/65**, 665 (1993).

[10] M. Brandbyge and P. Hedegård, Phys. Rev. Lett. **72**, 2919 (1994).

[11] K. Hirose and M. Tsukada, Phys. Rev. Lett. **73**, 150 (1994).

[12] R. Gomer, IBM J. Res. Dev. **30**, 426 (1986).

[13] U. Dürig, O. Züger, L. C. Wang, and H. J. Kreuzer, Europhys. Lett. **23**, 147 (1993).

[14] R. Hübner and G. Doyen, Surf. Sci. **178**, 813 (1986).

[15] S. Ciraci, in *Scanning Tunneling Microscopy III*, edited by R. Wiesendanger and H.-J. Güntherodt (Springer-Verlag, Berlin, 1993), p. 179.

[16] U. Dürig and O. Züger, Vaccum **41**, 382 (1990).

[17] D. Drakova, G. Doyen, and F. von Trentini, Phys. Rev. B **32**, 6399 (1985); G. Doyen and D. Drakova, Surf. Sci. **178**, 375 (1986); G. Doyen, D. Drakova, E. Kopatzki, and R. J. Behm, J. Vac. Sci. Technol. A **6**, 327 (1988); E. Kopatzki, G. Doyen, D. Drakova, and R. J. Behm, J. Microsc. (Oxford) **151**, 687 (1988); G. Doyen, E. Koetter, J. Barth, and D. Drakova, in *Basic Concepts and Applications of Scanning Tunneling Microscopy and Related Techniques*, edited by R. J. Behm *et al.* (Kluwer, Dordrecht, 1990), p. 97; D. Drakova and G. Doyen, Surf. Sci. **226**, 263 (1990); G. Doyen and D. Drakova, in *Quantum Chemistry Approaches to Chemisorption and Heterogeneous Catalysis*, edited by F. Ruette (Kluwer, Dordrecht, 1992), p. 139.

[18] D. Drakova, G. Doyen, and R. Hübner, J. Chem. Phys. **89**, 1725 (1988).

[19] M. E. Grillo, G. R. Castro, and G. Doyen, J. Phys. Condens. Matter **4**, 5103 (1992).

[20] R. M. Eastment and C. H. B. Mee, J. Phys. F **3**, 1738 (1973); J. Hölzl and F. K. Schulte, in *Solid Surface Physics*, edited by G. Höhler, Springer Tracts in Modern Physics (Springer, Berlin, 1979); V. L. Moruzzi, J. F. Janak, and A. R. Williams, *Calculated Electronic Properties of Metals* (Pergamon, New York, 1978); J. A. Bardeen and A. F. Burr, Rev. Mod. Phys. **39**, 125 (1967); J. C. Fuggle and N. Mårtensson, J. Electron Spectrosc. Relat. Phenom. **21**, 275 (1980); P. Steiner, H. Höchst, and S. Hüfner, Z. Phys. B **30**, 129 (1978); M. van Hove and S. Tong, Surf. Sci. **54**, 91 (1976); H. B. Nielsen and D. L. Adams, J. Phys. C **15**, 615 (1982); F. Jona, D. Sondericker, and P. M. Marcus, J. Phys. C **13**, L155 (1980); J. Schmit and A. A. Lucas, Solid State Commun. **11**, 419 (1972).

[21] A. D. McLean and R. S. McLean, At. Data Nucl. Data Tables **26**, 197 (1981).

[22] H. Basch and H. B. Gray, Theor. Chim. Acta **4**, 367 (1966).

[23] E. Clementi and C. Roetti, At. Data Nucl. Data Tables **14**, 177 (1974).

[24] D. M. Bylander and L. Kleinman, Phys. Rev. B **19**, 1534 (1984).

[25] G. Doyen, Surf. Sci. **122**, 505 (1982).

[26] K. Ruedenberg, Rev. Mod. Phys. **34**, 326 (1962).

[27] G. Doyen in *Scanning Tunneling Microscopy III*, edited by R. Wiesendanger and H.-J. Güntherodt (Springer-Verlag, Berlin, 1993), p. 23.

[28] D. Drakova and G. Doyen (unpublished).

[29] G. Ehrlich and C. F. Kirk, J. Chem. Phys. **48**, 1465 (1968); E. W. Plummer and T. N. Rhodin, *ibid*. **49**, 3479 (1968); T. T. Tsong and R. Casanova, Phys. Rev. B **21**, 4564 (1980); **24**, 3063 (1981); G. Ehrlich and F. G. Hudda, J. Chem. Phys. **44**, 1039 (1966); T. T. Tsong and G. Kellog, Phys. Rev. B **12**, 1343 (1975); J. R. Banavar, M. H. Cohen, and R. Gomer, Surf. Sci. **107**, 113 (1981); D. W. Basset and M. J. Parsley, Br. J. Appl. Phys. **2**, 13 (1969).

[30] R. Stumpf and M. Scheffler, Phys. Rev. Lett. **72**, 254 (1994); Surf. Sci. **307-309**, 501 (1994).

[31] P. J. Feibelman, Phys. Rev. Lett. **69**, 1568 (1992).

[32] J. Wintterlin, J. Wiechers, H. Brune, T. Gritsch, H. Höffer, and R. J. Behm, Phys. Rev. Lett. **62**, 59 (1989); H. Brune, Ph.D. thesis, Freie Universität Berlin, Berlin, 1992.

[33] J. K. Gimzewski and R. Möller, Phys. Rev. B **36**, 1284 (1987).

[34] S. Ciraci, A. Baratoff, and I. P. Batra, Phys. Rev. B **42**, 7618 (1990).

[35] E. Koetter, Ph.D. thesis, Technische Universität Berlin, Berlin, 1992.